PAPER

Check for updates

Enhanced thermostability of C_2-symmetrical bis(imino)pyridine-iron precatalysts for ethylene polymerisation *via* a hybrid steric strategy†

Shuangshuang Liu,[abc] Qiuyu Li,[bc] Qaiser Mahmood, [iD] *[b] Zhixin Yu,*[a] Yizhou Wang,[d] Ran Zhang,[bc] Geng Ren[d] and Wen-Hua Sun [iD] *[abd]

The poor performance of bis(arylimino)pyridyl iron precatalysts in ethylene polymerisation at high-temperature makes them less attractive as drop-in catalysts for existing ethylene polymerisation technologies. In this study, employing a one-pot template approach, a series of C_2-symmetric bis(imino) pyridine-iron precatalysts were prepared from 2,6-diacetylpyridine, ferrous chloride, and aniline derivatives (eight distinct anilines bearing various steric and electronic substituents) and were characterized by FT-IR spectroscopy, elemental analysis, and single-crystal X-ray diffraction. These precatalysts showed high catalytic activity at industrially relevant temperatures. *In situ* activation with either MAO or MMAO, these complexes exhibited high catalytic activities (on the order of 10^6–10^7 g_{PE} mol_{Fe}^{-1} h^{-1}) over a wide temperature range (30–100 °C) and produced high-molecular-weight polyethylene (M_w up to 433.1 kg mol^{-1}) with unimodal to bimodal molecular weight distributions. The polymerisation activity, polymer molecular weights, and dispersity are significantly dependent on the *ortho*-substituents of the N-bound phenyl groups. Less sterically hindered substituents favored higher catalytic activities, while more hindered substituents facilitated the formation of higher molecular weight polyethylene. Moreover, these C_2-symmetric precatalysts with hybrid steric hindrance exhibited exceptional activity for producing high-molecular-weight polyethylene, outperforming previously reported symmetrical analogues that showed little to no activity. DSC and NMR analyses confirmed a highly linear polyethylene microstructure with predominantly methyl end groups.

Introduction

The development of non-precious, iron-based homogeneous catalysts has attracted significant interest in both academia and industry for olefin polymerisation, owing to their high natural abundance and low cost.[1] In particular, their low environmental impact positions them as promising candidates for the sustainable synthesis of polyethylene.[2] Therefore, since the initial report of bis(imino)pyridine iron complexes as highly active precatalysts for ethylene polymerisation in 1998 (**A**, Chart 1),[3] this field has witnessed remarkable growth and innovation.[1,4] The recent advances in

[a] *School of Pharmaceutical Sciences, Changchun University of Chinese Medicine, Changchun 130117, China. E-mail: yuzx01@ccucm.edu.cn*
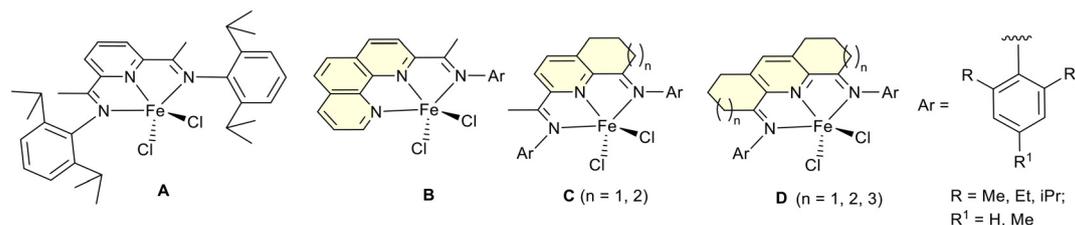[b] *Chemistry and Chemical Engineering Guangdong Laboratory, Shantou, 515031, China. E-mail: qaiser@ccelab.com.cn*
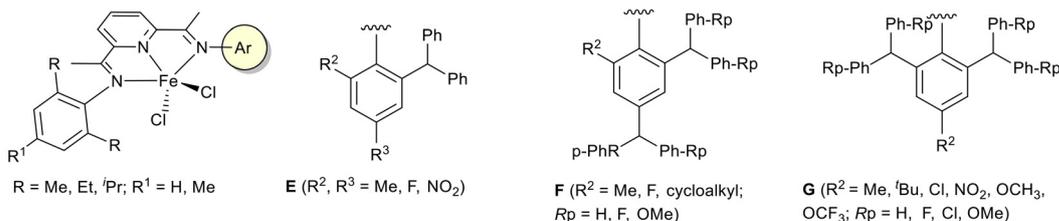[c] *AstaTech Biopharmaceutical Corporation, Chengdu 610095, China*
[d] *Key Laboratory of Engineering Plastics, Beijing National Laboratory for Molecular Sciences, Institute of Chemistry, Chinese Academy of Sciences, Beijing 100190, China. E-mail: whsun@iccas.ac.cn*
† Electronic supplementary information (ESI) available. See DOI: https://doi.org/10.1039/d5re00168d

ligand design have paved the way for synthesis of a variety of products, including selective volatile oligomers (C_4–C_{20}), long-chain α-macro-olefins (C_{20+}), and saturated low- to high-molecular-weight linear polyethylenes.[5] In particular, 2-imino-1,10-phenanthrolines-iron complex catalysts (**B**, Chart 1) have been recently applied at the industrial level for selective ethylene oligomerization (50 tons per year).[6]

Typically, the catalysis of ethylene polymerisation by bis(imino)pyridine-iron complexes is highly sensitive to changes in their ligand structure.[4,7] Variations in the ligand backbone commonly result in the formation of oligomers or low- to moderate-molecular-weight waxes accompanied by moderate to high polymerisation activities (**B–D**, Chart 1).[6,8–10] In particular, steric substituents at N-bound phenyl groups show pronounced influence on activity, chain transfer reactions and the properties of the resulting polyethylene.[11] Two types of steric approaches are commonly applied: unsymmetrical and symmetrical. The bis(imino) pyridine-iron complexes bearing two different N-bound aryl groups—one sterically less hindered and the other more hindered—serve as representative examples of the unsymmetrical steric approach (**E–G**, Chart 1). These catalysts

Chart 1 Variations in the ligand structure for synthesis of high performance iron precatalysts for ethylene polymerisation.

generate a hybrid steric environment at the axial coordination sites, exhibit high to exceptionally high activities (on the order of 10^6–10^7 g_{PE} mol_{Fe}^{-1} h^{-1}) across a wide temperature ra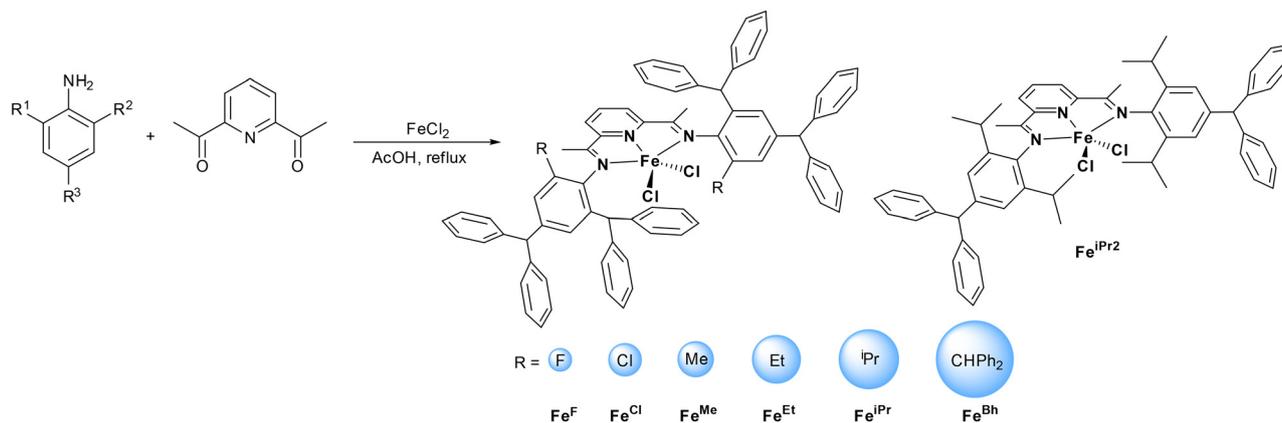nge (30–110 °C) and produce moderate- to high-molecular-weight polyethylene (M_w = 6.7–705 kg mol^{-1}) with a linear microstructure (**E–G**, Chart 1).[12–14] In contrast, complexes featuring identical N-bound aryl groups and a ligand backbone that is symmetrical on both sides of the metal centre are classified as symmetrical iron complexes (**A, D, H–I**, Fig. 1).[3,10,14e,h,15] Among them, those bearing sterically less hindered N-aryl groups exhibit significantly higher activity (**A** or **I**, Chart 1) than their more sterically encumbered counterparts (**H**, Chart 1). For instance, symmetrical iron complexes bearing benzhydryl groups were almost completely inactive yielding only trace amounts of polymer (**H**, Chart 1),[14e,h] while their sterically less bulky pentiptycenyl-substituted counterparts exhibited high activity (7.6 × 10^6 g_{PE} mol_{Fe}^{-1} h^{-1} at 80 °C) toward the production of low-molecular-weight polyethylene (M_n < 2500 g mol^{-1}) (**I**, Chart 1).[15] Moreover, unsymmetrical iron complexes outperform their symmetrical counterparts, as evidenced by benzosuberyl-substituted unsymmetrical iron complexes, which exhibit significantly higher activity (up to 25.3 × 10^6 g_{PE} mol_{Fe}^{-1} h^{-1} at 80 °C and 18.8 × 10^6 g_{PE} mol_{Fe}^{-1} h^{-1} at 100 °C) and produce polyethylene with higher molecular weights (up to 352.4 kg mol^{-1}),[14k]

reflecting enhanced catalytic efficiency and thermal stability over symmetrical analogues.[3,14e,h,15] These findings highlight the key influence of steric crowding around the metal centre in steering catalytic behaviour.[16] Precise modulation of steric congestion in symmetrical bis(imino)pyridine-iron complexes can enhance their polymerisation performance and control chain-growth dynamics at elevated temperature.

With the aim to improve the thermal stability with high activity, a series of C_2-symmetrical iron complexes were prepared using a hybrid steric approach (**J**, Chart 1): the complexes bear identical N-bound aryl groups, with each aryl ring carrying two sterically distinct *ortho*-substituents, resulting in an unsymmetrical steric environment around the metal centre.[10b,12c,16c–e] Those complexes achieved not only high activity (in the level of 10^6–10^7 g_{PE} mol_{Fe}^{-1} h^{-1}) across a wide temperature range of 30–100 °C, but also produced high-molecular-weight polyethylene (M_w up to 433.1 kg mol^{-1}) with unimodal to bimodal molecular weight distributions. Systematic examination of reaction conditions, including cocatalyst screening, cocatalyst amount, reaction temperature, and time, revealed significantly high thermal stability and robustness of these iron precatalysts under various conditions. Indeed, the obtained polymerisation activity and polyethylene molecular weights are substantially higher than those of previously reported symmetrical iron complexes.

This journal is © The Royal Society of Chemistry 2025

React. Chem. Eng., 2025, **10**, 2030–2042 | **2031**

Scheme 1 One pot synthesis route for iron complexes used for ethylene polymerisation.

Results and discussion

Synthesis and characterization of iron complexes

As shown in Scheme 1, all iron complexes investigated for ethylene polymerisation were prepared in good to high yields using a one-pot template method (Scheme 1).[10,17] In particular, a suspension of 2,6-diacetylpyridine, $FeCl_2$, and aniline (in glacial acetic acid) was refluxed for 10 hours. Eight distinct anilines bearing various steric and electronic substituents were used individually. During reflux, the solution gradually turned green. After solvent removal and washing, the corresponding eight iron complexes were isolated (yield: 60–86%). FTIR spectra confirmed the coordination of the organic framework to the metal centre. The $\nu(C=N)$ stretching vibrations appeared in the range of 1580–1602 cm^{-1}, consistent with

previously reported iron complexes.[14] Theoretical and experimental results of elemental analysis further verified the purity and successful formation of these complexes. Additionally, the molecular structures of Fe^F and Fe^{Bh} were confirmed by single-crystal X-ray diffraction analysis.

Single crystals of both iron complexes, Fe^F and Fe^{Bh}, were obtained by the slow diffusion of n-hexane and diethyl ether (v/v = 3 : 1) into their dichloromethane solution at room temperature under a nitrogen atmosphere. The ORTEP perspectives are presented in Fig. 1, while selected bond lengths and bond angles are summarized in Table 1. Both complexes crystallize in the $P2_1/c$ space group and the iron centre is coordinated within the N_3 pocket of the bisiminopyridine ligand, resulting in a five-coordinate geometry. The Fe^F complex adopts a distorted square

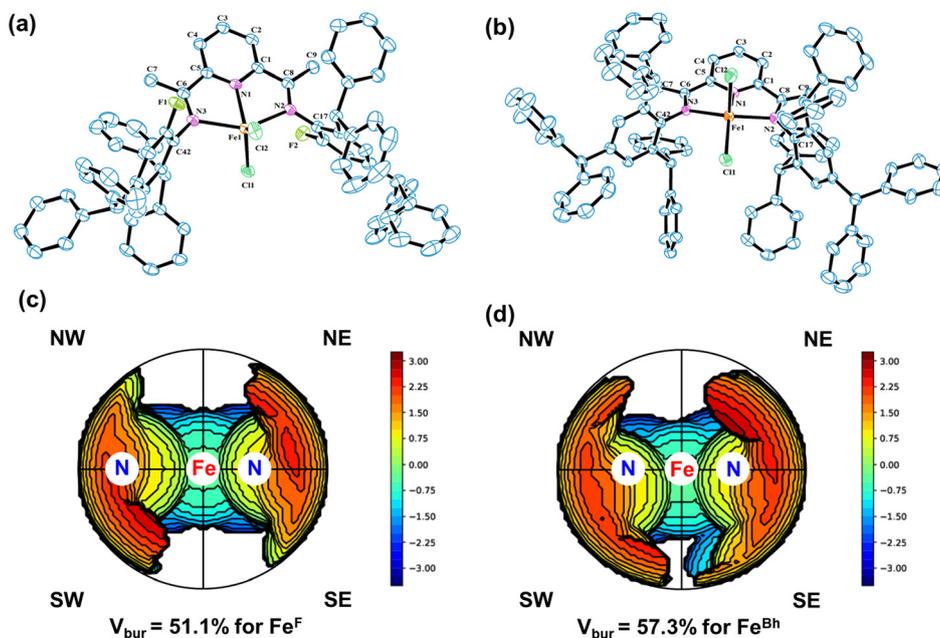**Fig. 1** Molecular structure of (a) Fe^F and (b) Fe^{Bh} with thermal ellipsoids shown at a 30% probability level. Disordered chloro groups in Fe^F, disordered phenyl ring in Fe^{Bh} and all hydrogen atoms are removed to make clear ORTEP view of the structure. Steric maps and V_{bur} were calculated by a DFT computational method (BP86-D3) for (c) Fe^F and (d) Fe^{Bh}.

Table 1 Selected bond lengths (Å) and angles (°) of Fe^F and Fe^{Bh}

	Fe^F	Fe^{Bh}
Bond length (Å)		
Fe(1)–Cl(1)	2.2871(8)	2.2512(15)
Fe(1)–Cl(2)	2.3015(8)	2.3252(16)
Fe(1)–N(3)	2.281(2)	2.225(4)
Fe(1)–N(2)	2.272(2)	2.238(4)
Fe(1)–N(1)	2.105(2)	2.083(4)
N(3)–C(42)	1.431(3)	1.428(6)
N(3)–C(6)	1.281(3)	1.303(6)
N(2)–C(8)	1.282(3)	1.284(6)
N(2)–C(17)	1.430(4)	1.444(6)
N(1)–C(5)	1.333(4)	1.352(6)
N(1)–C(1)	1.339(3)	1.340(6)
Bond angles (°)		
Cl(1)–Fe(1)–Cl(2)	121.50(4)	119.09(7)
N(3)–Fe(1)–Cl(2)	90.89(6)	98.55(11)
N(3)–Fe(1)–Cl(1)	105.13(6)	101.93(11)
N(1)–Fe(1)–Cl(2)	114.32(6)	92.41(12)
N(1)–Fe(1)–Cl(1)	124.18(6)	148.36(12)
N(1)–Fe(1)–N(3)	73.36(8)	74.15(15)
N(1)–Fe(1)–N(2)	73.29(8)	72.95(15)
N(2)–Fe(1)–Cl(2)	103.74(6)	99.05(11)
N(2)–Fe(1)–Cl(1)	92.66(6)	97.36(11)
N(2)–Fe(1)–N(3)	146.62(8)	143.10(14)

pyramidal geometry with some trigonal bipyramidal character ($\tau_5 = 0.374$), whereas Fe^{Bh} exhibits a nearly square pyramidal geometry with minimal trigonal bipyramidal distortion ($\tau_5 = 0.087$). The τ_5 distortion parameter is $\tau_5 = (\beta - \alpha)/60$, where β and α are the largest and second-largest X–M–X angles ($\tau_5 = 0$ for a perfect square pyramid, and $\tau_5 = 1$ for a perfect trigonal bipyramid).[18] Similar structural features have been reported for related iron complexes.[19] The difference in distortion between the two iron complexes arises primarily from variations in steric crowding around the metal centre. This is further reflected in the bite angles: Cl–Fe–Cl is 121.50° for Fe^F and 119.09° for Fe^{Bh}. The iron centre in Fe^{Bh} is slightly displaced (0.442 Å) from the plane of the three nitrogen atoms of the bisiminopyridine ligand, whereas in Fe^F, the iron and nitrogen atoms are nearly coplanar, reflecting minimal distortion. Additionally, the plane of the N-bound phenyl ring is nearly perpendicular to the pyridine plane, with dihedral angles of 78.44° and 76.40° for Fe^F, and 82.26° and 75.92° for Fe^{Bh}. The Fe–N1 bond length is slightly longer than the Fe–N2 and Fe–N3 bond lengths, indicating that the pyridine nitrogen exhibits stronger coordination than the imine nitrogen atoms. In Fe^F, the benzhydryl substituents at the *ortho* positions of the N-bound phenyl rings adopt a *trans*-arrangement, with one substituent positioned above and the other below the axial plane. This *trans*-ligand structure results in less bulky steric hindrance around the iron centre compared to Fe^{Bh}, as quantitatively calculated using DFT (BP86-D3) with the SambVac tool.[20,21] As shown in Fig. 1c and d, the buried volume (% V_{bur}) of Fe^{Bh} is 57.3, significantly larger than Fe^F (51.1). This difference in steric environment around the active species leads to higher activity for Fe^F toward ethylene polymerization (*vide infra*).

Catalytic evaluation for ethylene polymerisation

All prepared iron complexes were investigated for ethylene polymerisation. For comparison, a classical bisiminopyridine iron complex (**A**, Chart 1) was also tested under similar conditions.[3] In ethylene polymerisation, cocatalysts significantly influence catalyst activation and polymer properties.[12,22] Therefore, two cocatalysts, methyl aluminoxane (MAO) and modified methyl aluminoxane (MMAO), were chosen. Initially, reaction conditions (temperature, cocatalyst amount, and time) were optimized using the Fe^{Me} complex as the precatalyst with MAO and MMAO cocatalysts individually.

Screening of conditions with Fe^{Me}/MAO

To optimize the conditions under which Fe^{Me}/MAO displays the highest polymerisation activity, reaction parameters were systematically investigated (Table 2). Initially, the influence of reaction temperature on activity, polyethylene molecular weight, molecular weight dispersity, and melting point was examined, with results summarized in Table 2 (entries 1–8). Within the temperature range of 30 °C to 60 °C, polymerisation activity increased steadily. Fe^{Me} demonstrated outstanding performance across all temperatures, achieving the highest activity of 17.2×10^6 g mol^{-1} h^{-1} at 60 °C—a 112% increase compared to 30 °C (Table 2, entries 1–4). This identifies 60 °C as the optimal temperature for the highest polymerisation activity (Fig. 2a). However, this enhancement in activity coincided with a decline in molecular weight from 433.1 kg mol^{-1} at 30 °C to 160.4 kg mol^{-1} at 60 °C. The decline in molecular weight indicates less control over polymer chain growth, likely due to higher chain transfer reactions, consistent with previous reports on bis(imino) pyridine-iron precatalysts.[14a,23] Beyond 60 °C, the polymerisation activity dropped gradually. At 90 °C, the activity decreased to 2.9×10^6 g$_{PE}$ mol$_{Fe}$$^{-1}$ h^{-1} (Table 2, entry 7). Despite this reduction, a high activity at 90 °C highlights the catalyst's remarkable thermal stability. At 100 °C, the activity further decreased to 0.7×10^6 g$_{PE}$ mol$_{Fe}$$^{-1}$ h^{-1}, with molecular weight dropping significantly to 4.6 kg mol^{-1} (Fig. 2a). These results suggest that elevated temperatures accelerate catalyst deactivation which in turn reduces polymerisation efficiency.[11,24] Additionally, the lower solubility of ethylene at higher temperatures likely also contributes to the drop in activity.[25] Although the activity decreases with the rise of temperature, this catalytic system not only maintained a high activity of 2.9×10^6 g$_{PE}$ mol$_{Fe}$$^{-1}$ h^{-1} but also produced polyethylene with a high molecular weight of $29.2 \times$ kg mol^{-1} at industrially relevant temperature of 90 °C (Table 2, entry 7). GPC curve analysis (Fig. 2b) revealed that reaction temperature substantially affected molecular weight dispersity, transitioning from broad to narrow distributions and from bimodal to unimodal profiles with the increase of temperature. Gibson and Brookhart previously reported that the bimodal distribution in PE obtained from bis(imino)pyridine-iron catalysts arises from

This journal is © The Royal Society of Chemistry 2025

React. Chem. Eng., 2025, **10**, 2030–2042 | **2033**

Table 2 Ethylene polymerisation using iron complex **Fe^{Me}** with MAO under different conditions[a]

Entry	T (°C)	Al/Fe	t (min)	PE (g)	Act.[b]	M_w[c]	M_w/M_n[c]	T_m[d] (°C)
1	30	2000	30	8.2	8.2	433.1	18.7	137.6
2	40	2000	30	14.3	14.3	244.7	9.6	136.3
3	50	2000	30	17.2	17.2	166.1	9.4	136.9
4	60	2000	30	17.4	17.4	160.4	17.8	137.1
5	70	2000	30	9.1	9.1	97.5	17.3	131.5
6	80	2000	30	7.4	7.4	56.1	7.72	129.8
7	90	2000	30	2.9	2.9	29.2	5.4	119.8
8	100	2000	30	0.7	0.7	4.6	1.8	130.6
9	60	1000	30	0.3	0.3	497.4	3.8	133.4
10	60	1250	30	6.7	6.7	254.3	21.5	136.9
11	60	1500	30	10.1	10.1	171.5	19.1	135.7
12	60	1750	30	16.0	16.0	166.8	13.4	135.8
13	60	2250	30	13.6	13.6	118.5	9.6	134.5
14	60	2500	30	7.5	7.5	109.1	9.1	137.6
15	60	2000	5	5.7	34.4	95.6	14.1	133.6
16	60	2000	15	12.3	24.6	135.2	13.2	136.3
17	60	2000	45	20.9	13.9	184.0	18.6	135.2
18	60	2000	60	22.3	11.1	188.4	13.4	135.7

[a] Conditions: **Fe^{Me}** (2.0 μmol); co-cat. (MAO); solvent toluene (100 mL); ethylene (1 MPa). [b] Activity in units of × 10^6 g$_{PE}$ mol$_{Fe}$$^{-1}$ h^{-1}. [c] Measured using GPC, M_w in units of × 10^3 g mol^{-1}. [d] DSC results.

two distinct chain termination pathways: chain transfer to aluminium species and β-H transfer to the monomer or to the metal centre.[3,19] The low molecular weight fraction primarily results from chain transfer to aluminium, while the high molecular weight fraction is associated with β-H transfer to the monomer. As evident from the GPC curves, the high

Fig. 2 (a) The relationship of reaction temperature with activity and polyethylene molecular weights, and (b) GPC curves of polyethylene obtained at different temperatures.

molecular weight fraction gradually diminished while the low molecular weight fraction increased with the rise of temperature. At 30 and 40 °C, the high molecular weight fraction dominated. At 50 °C, both fractions were nearly equal. From 60 to 90 °C, the high molecular weight fraction progressively decreased, with the low molecular weight fraction becoming dominant. Finally, at 100 °C, only the low molecular weight fraction remained, displaying a narrow dispersity (PDI = 1.8). These observations suggest that high reaction temperature probably accelerates the facile termination of the polymeric chain through β-hydrogen migration to ethylene on the active species, which initiates new chains and forms lower molecular weight polyethylene. Thus, the competing chain-transfer pathways result in bimodal molecular weight distributions.[26,27]

With the temperature fixed at 60 °C, the MAO amount relative to **Fe^{Me}** was increased from 1000 to 2500, with increments of 250 per reaction (Table 2, entries 4, 9–14). The polymerisation activity gradually improved as the Al/Fe molar ratio was increased (Fig. 3a). At an Al/Fe ratio of 1000, the lowest activity was observed, indicating that the effective cocatalyst range had not been reached. The activity steadily improved with higher Al/Fe ratios, giving a peak activity of 17.4 × 10^6 g$_{PE}$ mol$_{Fe}$$^{-1}$ h^{-1} at a ratio of 2000. This represent a 5633% increase in activity compared to the ratio of 1000 (Table 2, entry 4). However, further increases in the Al/Fe ratio to 2250 and 2500 led to lower activities of 13.6 and 7.0 × 10^6 g$_{PE}$ mol$_{Fe}$$^{-1}$ h^{-1}, respectively. The molecular weights of PE decreased gradually from 497.4 kg mol^{-1} to 109.1 kg mol^{-1}, aligning with trends reported for classical bis(imino)pyridine-iron complexes (Fig. 3a).[12–14] This decline is attributed to higher cocatalyst concentrations, which promote chain transfer reactions and result in polyethylene with lower molecular weight. The GPC curves (Fig. 3b) show
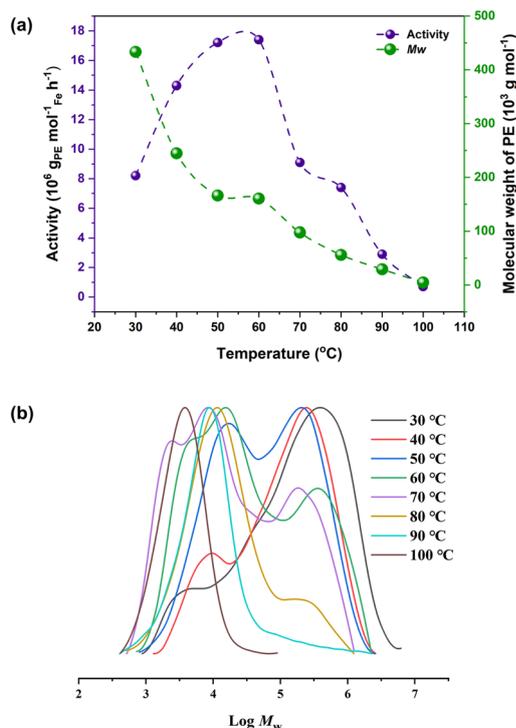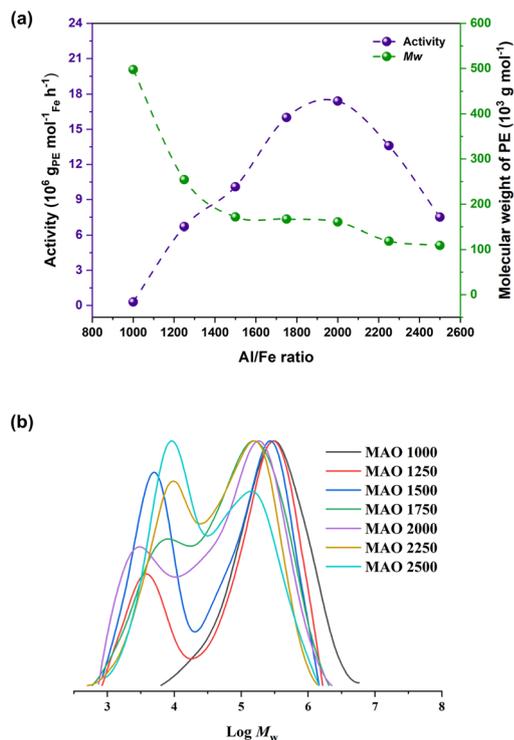
Fig. 3 (a) The relationship of different MAO amounts with activity and polyethylene molecular weights, and (b) GPC curves of polyethylene obtained at different MAO amounts.

a shift from unimodal to bimodal distributions with broader dispersity, supporting the correlation between cocatalyst concentration and molecular weight. The gradual increase in the low molecular weight fraction at higher cocatalyst concentrations further confirms that elevated cocatalyst levels accelerate chain transfer reactions. Consequently, this reduces chain propagation and yields polyethylene with lower molecular weight.[28]

To examine the stability of the **Fe^Me**/MAO catalytic system at 60 °C, a series of polymerisation tests were conducted at different reaction times in the range of 5 to 60 min under otherwise identical conditions and the results are summarized in Table 2 (entries 4, 15–18). The catalytic system was extremely active, producing 5.7 g of polyethylene in just 5 min with an activity of 34.4×10^6 g_{PE} mol_{Fe}^{-1} h^{-1} (Table 2, entry 15). This indicates that only a short induction period was required to generate the maximum number of active species for polymerisation. Prolongation of the reaction time led to a gradual increase in both polyethylene yield and molecular weight. The polymer yield increased from 5.7 g to 22.3 g, while the molecular weight increased from 95.6 kg mol^{-1} to 188.4 kg mol^{-1}. This steady rise in yield and molecular weight strongly suggests that the polymerisation species remained active over prolonged reaction times, highlighting the high stability of the catalytic system. However, the polymerisation activity gradually declined from 34.4×10^6 to 11.1×10^6 g_{PE} mol_{Fe}^{-1} h^{-1} with extended reaction time (Table 2, entries 4, 15–18), likely due

to the partial decomposition of active species and/or polymer mass removal problems.[14] The continuous increase in polymer yield over time reduces ethylene concentration in the reaction medium, which in turn ultimately affects the overall polymerisation activity. The molecular weight dispersity of the obtained polyethylene remained broad and bimodal (Fig. S5†). At reaction times of 5 and 10 minutes, low-molecular-weight polyethylene was the predominant fraction, accompanied by a less intense high-molecular-weight peak. With prolongation of reaction time, the peak of high-molecular-weight fraction gradually increased until it matched that of the low-molecular-weight fraction. These results indicate that, at the onset of polymerisation, two active species contributed to chain propagation: one more prone to chain transfer reactions, producing the low-molecular-weight fraction, while the other likely exhibited living polymerisation behaviour, leading to a continuous increase in the high-molecular-weight fraction over time. In conclusion, the catalytic system demonstrated high stability over extended reaction times, producing high-molecular-weight polyethylene with bimodal dispersity and high melt temperatures (T_m = 133.6–137.1 °C).

Screening of conditions with Fe^Me/MMAO

Further polymerisation tests were conducted to examine the impact of replacing the cocatalyst with MMAO. These tests were performed using **Fe^Me** with MMAO at different temperatures and cocatalyst concentrations, with the results presented in Table 3. As expected, the increase of the reaction temperature from 30 °C to 40 °C and subsequently to 60 °C led to a linear rise in polymerisation activity, from 4.9×10^6 to 18.7×10^6 g_{PE} mol_{Fe}^{-1} h^{-1} (Table 3, entries 1–3). Possibly, the facile N-aryl rotation at higher temperatures reduces the steric hindrance around the active species.[14] This facilitates monomer access to the active site and thereby improves coordination and insertion efficiency. However, further reaction at higher temperatures of 80 °C to 100 °C resulted in a linear decline in activity, giving a minimum value of 0.7×10^6 g_{PE} mol_{Fe}^{-1} h^{-1} at 100 °C (Table 3, entries 4–5). The decomposition of the active species and reduced solubility of ethylene in the reaction medium at higher temperature likely decrease the activity,[24,25] a trend that closely mirrors the observations made with MAO. Consistent with the typical behaviour of iron complexes in ethylene polymerisation, the polymer molecular weight decreased from 108.7 kg mol^{-1} to 2.6 kg mol^{-1} as the temperature increased from 30 °C to 100 °C, representing an approximate 97.6% decrease. Higher chain transfer reactions at higher temperatures decrease the molecular weight of resulting polyethylene.[26,27] The molecular weight distributions transitioned from bimodal to unimodal, similar to the trend observed with MAO. As evident from the GPC curves (Fig. S1†), a broad bimodal distribution was observed at reaction temperatures of 30 °C and 40 °C. Beyond this temperature range, the high-molecular-weight peak gradually disappeared, leaving only a

This journal is © The Royal Society of Chemistry 2025

React. Chem. Eng., 2025, **10**, 2030–2042 | **2035**

Table 3 Ethylene polymerisation using iron complex **Fe^Me** with MMAO under different conditions[a]

Entry	T (°C)	Al/Fe	Time (min)	PE (g)	Act.[b]	M_w[c]	M_w/M_n[c]	T_m[d] (°C)
1	30	2000	30	4.9	4.9	108.7	20.8	131.1
2	40	2000	30	7.9	7.9	27.1	5.9	132.4
3	60	2000	30	18.7	18.7	18.6	1.8	131.9
4	80	2000	30	8.3	8.3	11.5	1.6	129.3
5	100	2000	30	0.7	0.7	2.6	1.2	125.7
6	60	1000	30	14.6	14.6	283.9	7.3	135.7
7	60	1500	30	16.8	16.8	46.9	2.6	133.9
8	60	2500	30	16.4	16.4	16.3	1.9	131.3

[a] Conditions: **Fe^Me** (2.0 μmol); co-cat. (MMAO); solvent toluene (100 mL); ethylene (1 MPa). [b] Activity in units of × 10⁶ g_{PE} mol_{Fe}^{-1} h^{-1}. [c] Measured using GPC, M_w in units of × 10³ g mol⁻¹. [d] DSC results.

low-molecular-weight peak. Therefore, a unimodal dispersity was observed at higher temperatures (80–100 °C). The disappearance of the high-molecular-weight fraction is likely due to increased chain termination *via* β-H elimination, an indication of single-site catalytic behaviour at elevated temperatures. The high melting points of obtained polyethylene (131.1–125.7 °C) indicate a highly linear microstructure, further validated by high-temperature NMR analysis (*vide infra*).

Further, the polymerisation activity and polymer properties were examined at different Al/Fe molar ratios of 1000, 1500, 2000, and 2500 to identify the optimal cocatalyst concentration (Table 3, entries 3, 6–8). The results indicate a clear correlation between cocatalyst concentration and polymerisation performance, with the highest activity observed at an Al/Fe ratio of 2000, beyond which further increases in cocatalyst led to a decline in activity. The polymerisation activity increased by approximately 28% as the Al/Fe ratio increased from 1000 to 1500, reaching a peak activity of 18.7 × 10⁶ g_{PE} mol_{Fe}^{-1} h^{-1} at an Al/Fe ratio of 2000. However, polymerisation at 2500 caused a decrease in activity, with a reduction of about 12% compared to the peak

value at 2000 (Table 4, entry 8). The molecular weights showed a notable decline with the increase of cocatalyst concentration, a trend also observed in MAO based polymerisation. It dropped by around 83% from 283.9 kg mol⁻¹ (Al/Fe = 1000) to 16.3 kg mol⁻¹ (Al/Fe = 1000). It is again assumed that higher cocatalyst concentrations promote chain transfer reactions, resulting in lower molecular weight polyethylene.[28] Molecular weight distributions remained unimodal but broad at low cocatalyst concentrations (Fig. S2†) and became narrower at higher concentrations (PDI = 7.3–1.8). The melting point temperatures ranged from 131.3 to 135.7 °C, depending on polymer molecular weight.

Screening of ligand structure using MAO or MMAO as a cocatalyst

All the iron complexes were tested to explore the steric and electronic effects of *ortho*-substituents on ligands (Scheme 1), with comparisons made to the classical Brookhart's iron precatalyst under identical conditions (**A**, Chart 1).[3] The polymerisation experiments were conducted under optimal conditions [temperature = 60 °C and = Al/Fe ratio = 2000] and

Table 4 Ethylene polymerisation using different iron complexes with MAO or MMAO under similar conditions[a]

Entry	Precat.	Co-cat.	PE (g)	Act.[b]	M_w[c]	M_w/M_n[c]	T_m[d] (°C)
1	**Fe^F**	MAO	10.7	10.7	36.6	4.1	132.1
2	**Fe^Cl**	MAO	12.8	12.8	116.2	22.5	136.8
3	**Fe^Me**	MAO	17.4	17.4	160.4	17.8	137.1
4	**Fe^Et**	MAO	11.3	11.3	177.7	13.6	134.5
5	**Fe^iPr**	MAO	1.7	1.7	483.6	3.6	133.2
6	**Fe^iPr2**	MAO	6.3	6.3	6.2	4.8	133.8
7	**Fe^Bh**	MAO	0.1	0.1	3.5	2.2	129.6
8	**A**	MAO	8.7	8.7	2.5	1.6	132.9
9	**Fe^F**	MMAO	15.6	15.6	56.3	4.4	129.9
10	**Fe^Cl**	MMAO	11.2	11.2	17.9	3.7	133.5
11	**Fe^Me**	MMAO	18.7	18.7	18.6	1.8	131.9
12	**Fe^Et**	MMAO	12.3	12.3	71.7	4.7	136.7
13	**Fe^iPr**	MMAO	3.4	3.4	270.8	12.4	133.1
14	**Fe^iPr2**	MMAO	4.9	4.9	4.3	1.9	131.3
15	**Fe^Bh**	MMAO	0.1	0.1	4.3	1.8	126.5
16	**A**	MMAO	6.7	6.7	103.7	9.0	132.0

[a] Conditions: iron complexes (2.0 μmol); cocatalysts (Al/Fe = 2000); solvent toluene (100 mL); temperature (60 °C); time (30 min); ethylene (1 MPa). [b] Activity in units of × 10⁶ g_{PE} mol_{Fe}^{-1} h^{-1}. [c] Measured using GPC, M_w in units of × 10³ g mol⁻¹. [d] DSC results.
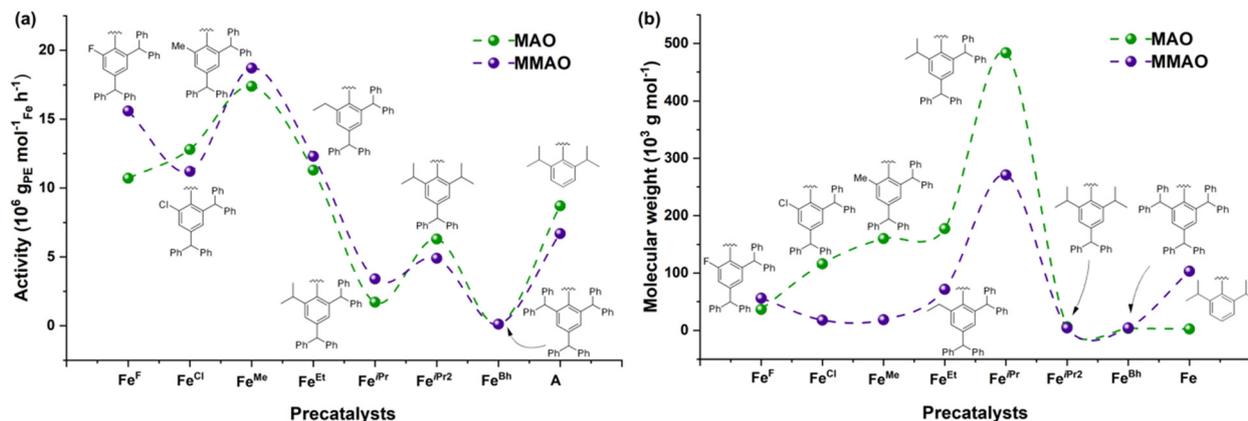
Fig. 4 The relationship of ligand structure with (a) activity and (b) polyethylene molecular weights under identical conditions.

results are summarized in Table 4 (entries 1–16). As illustrated in Fig. 4, variations in the steric and electronic properties of the *ortho*-substituents led to distinct trends in polymerisation activity and polyethylene molecular weights.

Iron complexes with MAO. To examine the electronic effects, the polymerisation performance of iron complexes **Fe^F** (R = F), **Fe^Cl** (R = Cl), and **Fe^Me** (R = Me) was compared under similar conditions (Table 4, entries 1–3). The **Fe^F** complex, with the fluoro electron-withdrawing substituent (R = F), exhibited an activity of 10.7×10^6 g_{PE} mol_{Fe}^{-1} h^{-1} (Table 4, entry 1, Fig. 4a). This activity is approximately 16% lower than that of **Fe^Cl** bearing a relatively weaker electron-withdrawing substituent (R = Cl), while significantly lower, about 38%, than that of **Fe^Me** containing an electron-donating substituent (R = Me). Following the same trend of activity, the molecular weight of polyethylene showed an almost linear increase as the *ortho*-substituent changed from strong electron-withdrawing (F) to less electron-withdrawing (Cl) and then to electron-donating (Me) (Fig. 4b). The relatively higher catalytic activity of **Fe^Me** can be attributed to several factors. The electron-donating nature of the methyl group likely stabilizes the metal centre.[29] Moreover, the *ortho*-methyl substituent likely enhances the solubility of the precatalyst compared to others, which also contributes to improved polymerisation activity.[14e,h] On the other hand, strong electron-withdrawing groups, such as F or Cl substituents, may interact with the β-H on the growing polymer chain, promoting chain transfer and resulting in lower molecular weight polyethylene.[30] Overall, these factors combine to increase the activity and polymer molecular weight for **Fe^Me**. The polymer molecular weight distributions were broad, ranging from unimodal to bimodal (Fig. S3†). The high molecular weight fraction dominated in **Fe^Me**-based polyethylene with broad dispersity (M_w/M_n = 17.8), whereas the opposite trend was observed in **Fe^Cl**-based polyethylene (M_w/M_n = 22.5). In **Fe^F**, the distribution was broad but unimodal. These results highlighted the presence of multi-site active species or different modes of chain termination reactions.

The steric effects were then investigated for the iron complexes **Fe^Me** (R = Me), **Fe^Et** (R = Et), **Fe^iPr** (R = iPr), **Fe^iPr2** (R = iPr2), **Fe^Bh** (R = CHPh₂), and **A** under identical conditions

(Table 4, entries 3–8). A detailed analysis of the results revealed a strong correlation between polymerisation activity, molecular weights, and the steric hindrance of *ortho*-substituents. Generally, less sterically hindered precatalysts favoured higher polymerisation activity, while more hindered complexes tended to produce higher molecular weight polyethylene (Fig. 4a).[14] For example, changing the *ortho*-methyl substituent in **Fe^Me** with the bulkier ethyl group in **Fe^Et** decreased the catalytic activity by 35%, from 17.4×10^6 to 11.3×10^6 g_{PE} mol_{Fe}^{-1} h^{-1} (entries 4 *vs.* 4). A more significant drop in activity, about 90% compared to **Fe^Me** and 85% compared to **Fe^Et**, occurred when isopropyl was introduced in **Fe^iPr**. The negative impact of steric hindrance became even more evident when the bulky *ortho*-benzhydryl group in **Fe^iPr** was replaced by the smaller isopropyl group in **Fe^iPr2**. This decrease in steric hindrance resulted in a 270% increase in activity. On the other hand, changing both *ortho*-isopropyl groups with benzhydryl groups in **Fe^Bh** nearly shut down the polymerisation, yielding only a small amount of polymer (100 mg). The activity of these iron complexes can be arranged in the order of increasing steric hindrance: **Fe^Me** (R = Me) > **Fe^Et** (R = Et) > **Fe^iPr2** (R = iPr2) > **Fe^iPr** (R = iPr) > **Fe^Bh** (R = CHPh₂). The polymerisation activity decreased almost linearly with the increase of steric hindrance. This trend can be attributed to the fact that less sterically hindered complexes allow more efficient coordination and monomer insertion into the active site for high polymerisation activity. In contrast, bulkier substituents hinder access to the metal centre which reduces activity. On the other hand, molecular weights of the obtained polyethylene improved with the increase of steric hindrance for **Fe^Me**, **Fe^Et**, and **Fe^iPr** (Fig. 4b). The PE produced by **Fe^Me** had a molecular weight of 160.4 kg mol⁻¹, which increased by 10% to 177.7 kg mol⁻¹ for **Fe^Et**, and by 170% to 483.6 kg mol⁻¹ for **Fe^iPr**. Increased steric hindrance around the active species favors chain propagation over chain transfer reactions, thus resulting in higher molecular weights.[14e,h,16,31] The consistent decrease in molecular weight dispersity from 17.8 to 3.6 further supports these findings (Fig. S3†). However, excessive steric hindrance can hinder monomer access to the active species, reducing both activity and molecular weights, as observed with **Fe^Bh**.

Under similar conditions, the classical Brookhart precatalyst (**A**, Chart 1) exhibited significantly lower polymerisation activity and molecular weight compared to the prepared precatalysts, particularly Fe^{Me} (Fig. 4).[3] However, it showed slightly better results than Fe^{iPr2}. These comparative results highlight the importance of balancing steric hindrance to achieve high polymerisation activity and desirable polymer properties.

Iron complexes with MMAO. In combination with MMAO, the prepared iron complexes were tested for ethylene polymerisation to assess the effect of the cocatalyst on the catalytic performance and the structure–activity relationship. The results are presented in Table 4 (entries 9–16). Overall, the observed structure–activity trends are similar to those seen with MAO activation. For instance, among Fe^F, Fe^{Cl}, and Fe^{Me} (Table 4, entries 9–11), Fe^{Me} exhibited slightly higher activity than Fe^F and Fe^{Cl}, whereas the molecular weight of the obtained polyethylene followed the opposite trend (Fig. 4). This confirms that complexes bearing electron-donating substituents enhance the catalytic activity compared to those with electron-withdrawing groups but result in polyethylene with lower molecular weight, highlighting the strong influence of electronic effects on catalytic performance.

The iron complexes with excessive steric hindrance at the *ortho* position exhibit reduced catalytic activity but increased polyethylene molecular weights, a trend also observed with MAO (Fig. 4). For example, the increase of steric bulk of the substituent from methyl (Fe^{Me}) to ethyl (Fe^{Et}) and then to isopropyl (Fe^{iPr}) resulted in a linear increase in molecular weight of PE but a corresponding decline in activity (Table 4, entries 11–13). This trend is further evident when comparing the performance of Fe^{iPr2}, Fe^{iPr}, and Fe^{Bh} (Table 4, entries 13–15). Complex Fe^{Bh}, with benzhydryl groups at all four *ortho* positions, produced an almost negligible amount of polymer (100 mg) with very low activity (0.1×10^6 g_{PE} mol_{Fe}^{-1} h^{-1}, entry 15). Replacement of all benzhydryl with sterically less hindered *ortho*-isopropyl groups in Fe^{iPr2} gave a much higher activity up to 4.9×10^6 (entry 15). As expected, the Fe^{iPr} complex bearing two benzhydryl and two isopropyl groups—imparting steric congestion between Fe^{Bh} and Fe^{iPr2}—displayed slightly lower activity than Fe^{iPr2} but significantly surpassed Fe^{Bh} (entry 14). However, the opposite trend was observed for polymer molecular weight with the increase of steric hindrance, with 4.3 kg mol^{-1} for the sterically less hindered complex, Fe^{iPr2} and 270.8 kg mol^{-1} for the sterically more hindered complex, Fe^{iPr}. Increased steric hindrance around the active species restricts monomer access, which lowers activity. However, it also prevents chain transfer reactions, resulting in higher polymer molecular weight.[14e,h,16,31] This emphasizes the key role of steric hindrance in catalytic performance. As shown in Fig. S4,† the molecular weight dispersity of the obtained polyethylene remained unimodal, ranging from narrow to broad (M_w/M_n = 1.8–4.7) across all the iron complexes, except for polyethylene produced with Fe^{iPr}, which exhibited a significantly broader and bimodal dispersity with (M_w/M_n = 12.4). The Fe^{iPr} complex, bearing bulky isopropyl groups, likely imposes greater restrictions on *N*-aryl rotation compared to other iron complexes, potentially leading to the formation of two isomers: *rac* and *cis*.[32] These distinct isomers, with varying steric hindrance at axial sites, resulted in polyethylene with bimodal molecular weight dispersity, characterized by a dominant high-molecular-weight fraction (Fig. S4†). Similar to MAO-based studies, Brookhart's classical iron precatalyst (**A**, Chart 1) exhibited considerably lower activity than Fe^F, Fe^{Cl}, Fe^{Me}, and Fe^{Et} but slightly higher than Fe^{iPr} and Fe^{iPr2} and produced polyethylene with a molecular weight of 103.7 kg mol^{-1} (M_w/M_n = 9.0), significantly lower than Fe^{iPr}-based polyethylene, but higher than those obtained with other iron complexes. This discrepancy primarily arises from differences in steric and electronic substituents.

Moreover, comparative studies of both cocatalysts under similar conditions revealed that these iron complexes exhibited slightly higher activity when activated with MMAO (Fig. 4). However, polyethylene produced using MAO-activated iron complexes displayed relatively higher molecular weights with unimodal to bimodal dispersity. These variations in polymerisation outcomes likely stem from differences in the activation process and cocatalyst sizes.[15,33] Overall, MAO-based polymerisation demonstrated superior activity at 60 °C, whereas MMAO-based polymerisation yielded polyethylene with higher molecular weights but less control over dispersity.

Microstructural and thermal properties

The melt temperature of linear polyethylene is mainly dependent on its molecular weight.[4] Changes in the reaction conditions, especially the reaction temperature, significantly affect the polymer molecular weights and melt temperatures. The melt temperature of polyethylene decreased from 137.6 °C to 119.8 °C in the case of Fe^{Me}/MAO-based polymerisation and from 132.4 °C to 125.7 °C in the case of Fe^{Me}/MMAO-based polymerisation with the increase of the reaction temperature. This decline in melt temperature is likely due to the decreased molecular weight of polyethylene with the elevation of reaction temperature. Overall, the melt temperatures remained high (generally over 130 °C) across all reaction conditions. Such high melting temperatures indicate a highly linear structure of the obtained polyethylene. To further confirm the structure of the polyethylene, high-temperature $^1H/^{13}C$ NMR measurements were performed for selected polyethylene samples prepared at 30 °C and 100 °C. The ^1H and ^{13}C NMR spectra of polyethylene obtained at 100 °C are shown in Fig. 5 and 6, respectively. The peak assignments were based on previously reported work.[34] In the ^1H NMR spectrum, an intense peak (H_{IV}) appeared at δ 1.31 ppm, which is the characteristic signal of the CH_2 repeating unit in the polymer chain. The peak (H_{VII}) at δ 0.91 ppm corresponds to the methyl end group, while two less intense multiplet peaks (H_{II} and H_I) at δ 5.83 ppm and 5.02 ppm (intensity ratio 1:2) were attributed to vinyl end groups (–CH=CH$_2$). Additionally, a weak peak (H_{III}) at δ
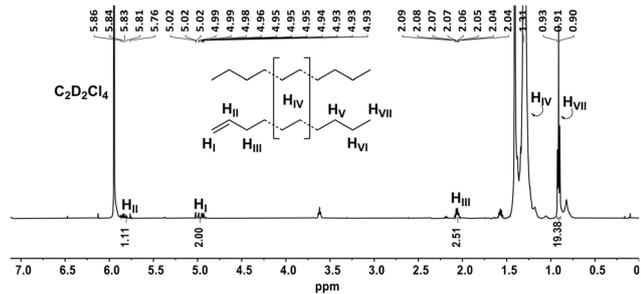
2038 | *React. Chem. Eng.*, 2025, **10**, 2030–2042

This journal is © The Royal Society of Chemistry 2025

Fig. 5 ^{1}H NMR spectrum of the PE sample obtained with **Fe^{Me}**/MAO at 100 °C (Table 2, entry 8).
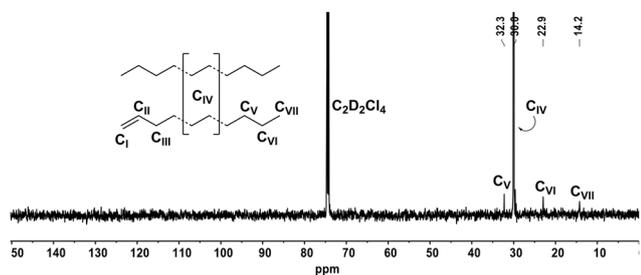
Fig. 6 ^{13}C NMR spectrum of the PE sample obtained with **Fe^{Me}**/MAO at 100 °C (Table 2, entry 8).

2.07 ppm was assigned to protons adjacent to the vinyl groups. In the ^{13}C NMR spectrum of the same sample, the corresponding peaks for C_{VII}, C_{VI}, C_{IV} and C_V appeared at δ 14.2 ppm, 22.9 ppm, 30.0 ppm and 32.3 ppm respectively. The C_I and C_{II} signals were not observed in the ^{13}C NMR spectrum due to the low solubility of the polyethylene sample. The relative integration of protons from the methyl chain end and the CH_2 of the vinyl chain end revealed that chain termination reactions proceed through both β-H elimination and chain transfer to aluminium species. The amount of methyl chain ends was relatively higher than that of vinyl chain ends (saturated PE chains = 73%), indicating that chain transfer to aluminium species is the primary pathway for chain termination. Moreover, the ^{1}H and ^{13}C NMR spectra of polyethylene obtained at 30 °C did not show peaks for vinyl bonds (Fig. S20 and S21†), indicating that chain termination reactions occur only through chain transfer to aluminium species. This suggests that β-H elimination reactions occur at higher polymerisation temperatures. As the temperature rises, the elimination reaction is increasingly favored over chain transfer to the aluminium reagent.

Experimental

Synthesis of iron complexes

Following the general procedure described for the synthesis of **Fe^{Me}**, all the iron complexes were prepared in good to excellent yields.

Fe^{Me} (general procedure). Under a nitrogen atmosphere, 2,6-diacetylpyridine (1.0 mmol), aniline (2.0 mmol), and FeCl$_2$ (1.0 mmol) were added to a 100 mL round-bottom flask, followed by the addition of 15 mL of acetic acid. The reaction mixture was heated to 120 °C with constant magnetic stirring. The solution turned green within about 10 minutes. After 10 hours of heating and stirring, the mixture was filtered. The solvent of the filtrate was removed under reduced pressure, and the resulting precipitate was washed three times with *n*-hexane and recrystallized with dichloromethane to afford a green solid powder (0.76 g, 67%). FTIR (KBr, cm^{-1}): 3082 (w), 3058 (m), 3024 (m), 2916 (w), 2870 (w), 1642 ($v_{(C=N)}$, m), 1597 (s), 1493 (s), 1470 (m), 1449 (s), 1295 (w), 1264 (m), 1213 (m), 1184 (w), 1155 (w), 1139 (w), 1078 (m), 1031 (m), 914 (w), 891 (w), 807 (w), 770 (w), 745 (m), 700 (s), 632 (w), 619 (w). Anal. cacld. for C$_{75}$H$_{63}$Cl$_2$FeN$_3$ (1133.09) + CH$_3$COOH + H$_2$O: C, 76.36; H, 5.74; N, 3.47. Found: C, 76.67; H, 4.94; N, 3.38.

Fe^F. Following an identical procedure and reactant ratios to those used for **Fe^{Me}**, **Fe^F** was obtained as a green solid powder (0.49 g, 86%). FTIR (KBr, cm^{-1}): 3084 (w), 3060 (w), 3025 (m), 2961 (w), 2920 (w), 1619 ($v_{(C=N)}$, m), 1598 (w), 1494 (s), 1450 (m), 1428 (m), 1079 (m), 1031 (m), 914 (w), 879 (w), 833 (w), 773 (w), 745 (m), 701 (s), 633 (w), 619 (w). Anal. cacld. for C$_{73}$H$_{57}$Cl$_2$F$_2$FeN$_3$ (1141.02) + 2CH$_3$COOH + CH$_2$Cl$_2$: C, 69.60; H, 5.02; N, 3.12. Found: C, 69.53; H, 4.67; N, 3.48.

Fe^{Cl}. Following an identical procedure and reactant ratios to those used for **Fe^{Me}**, **Fe^{Cl}** was obtained as a green solid powder (0.47 g, 80%). FTIR (KBr, cm^{-1}): 3083 (w), 3059 (m), 3025 (m), 2920 (w), 1698 (w), 1621 ($v_{(C=N)}$, m), 1598 (s), 1557 (w), 1594 (s), 1449 (s), 1416 (w), 1302 (w), 1265 (m), 1222 (w), 1181 (w), 1155 (w), 1104 (w), 1078 (m), 1031 (m), 922 (w), 890 (w), 845 (w), 810 (m), 772 (m), 744 (m), 701 (s), 626 (w), 617 (w). Anal. cacld. for C$_{73}$H$_{57}$Cl$_4$FeN$_3$ (1173.93) + 3CH$_2$Cl$_2$ + H$_2$O: C, 63.10; H, 4.53; N, 2.90. Found: C, 63.42; H, 4.51; N, 3.12.

Fe^{Et}. Following an identical procedure and reactant ratios to those used for **Fe^{Me}**, **Fe^{Et}** was obtained as a green solid powder (0.65 g, 72%). FTIR (KBr, cm^{-1}): 3082 (w), 3059 (m), 3024 (s), 2967 (m), 2932 (w), 2875 (w), 1635 ($v_{(C=N)}$, w), 1598 (s), 1494 (s), 1449 (s), 1426 (w), 1371 (m), 1322 (w), 1267 (s), 1211 (m), 1185 (w), 1031 (m), 913 (w), 896 (w), 847 (w), 784 (w), 745 (m), 700 (s), 630 (w), 618 (w). Anal. cacld. for C$_{77}$H$_{67}$Cl$_2$FeN$_3$ (1161.15) + CH$_2$Cl$_2$ + 2H$_2$O: C, 73.07; H, 5.74; N, 3.28. Found: C, 73.02; H, 5.29; N, 3.14.

Fe^{iPr}. Following an identical procedure and reactant ratios to those used for **Fe^{Me}**, **Fe^{iPr}** was obtained as a green solid powder (0.81 g, 68%). FTIR (KBr, cm^{-1}): 3083 (w), 3059 (m), 3024 (m), 2962 (m), 2925 (w), 1599 ($v_{(C=N)}$, s), 1581 (s), 1494 (s), 1448 (s), 1371 (s), 1272 (s), 1211 (m), 1077 (m), 1031 (s), 956 (w), 897 (w), 848 (w), 805 (m), 782 (m), 742 (s), 701 (s), 631 (w), 618 (w). Anal. cacld. for C$_{79}$H$_{71}$Cl$_2$FeN$_3$ (1189.20) + CH$_2$Cl$_2$: C, 75.41; H, 5.78; N, 3.30. Found: C, 75.53; H, 5.82; N, 3.91.

Fe^{iPr2}. Following an identical procedure and reactant ratios to those used for **Fe^{Me}**, **Fe^{iPr2}** was obtained as a green solid powder (0.42 g, 64%). FTIR (KBr, cm^{-1}): 3082 (w), 3058

This journal is © The Royal Society of Chemistry 2025

React. Chem. Eng., 2025, **10**, 2030–2042 | **2039**

(m), 3025 (m), 2964 (s), 2929 (m), 2870 (m), 1585 ($v_{(C=N)}$, m), 1519 (s), 1494 (s), 1448 (s), 1385 (w), 1365 (m), 1259 (w), 1116 (w), 1075 (m), 1031 (m), 963 (w), 894 (m), 738 (m), 701 (s), 658 (w), 635 (w). Anal. cacld. for $C_{59}H_{63}Cl_2FeN_3$ (940.92) + $CH_3COOH + CH_2Cl_2 + H_2O$: C, 67.46; H, 6.48; N, 3.81. Found: C, 67.53; H, 6.85; N, 3.31.

Fe^{Bh}. Following an identical procedure and reactant ratios to those used for **Fe^{Me}**, **Fe^{Bh}** was obtained as a green solid powder (0.70 g, 60%). FTIR (KBr, cm^{-1}): 3082 (w), 3058 (m), 3024 (m), 1697 (w), 1645 ($v_{(C=N)}$, w), 1599 (m), 1540 (w), 1494 (s), 1447 (s), 1371 (m), 1266 (s), 1077 (m), 1031 (m), 910 (w), 874 (w), 768 (m), 749 (m), 700 (s), 606 (m). Anal. cacld. for $C_{99}H_{79}Cl_2FeN_3$ (1437.49) + H_2O: C, 81.70; H, 5.61; N, 2.89. Found: C, 82.08; H, 5.54; N, 2.88.

Conclusion

In summary, a hybrid steric approach was investigated in C_2-symmetric bis(imino)pyridine-iron complexes for ethylene polymerisation. The *ortho*-substituents of the N-bound phenyl group were systematically varied with different steric and electronic substituents. The variation in the steric substituents significantly influenced the coordination sphere and buried volume, which in turn affected the catalytic performance in ethylene polymerisation. Upon *in situ* activation with either MAO or MMAO, the sterically less hindered iron complexes exhibited exceptionally high activities (up to 18.7×10^6 g_{PE} mol_{Fe}^{-1} h^{-1} at 60 °C) and maintained a high activity of 2.9×10^6 g_{PE} mol_{Fe}^{-1} h^{-1} even at an elevated temperature of 90 °C. On the other hand, the sterically more hindered iron precatalysts facilitated chain growth for high-molecular-weight polyethylene (M_w up to 433.1 kg mol^{-1}) with unimodal to bimodal molecular weight distributions. Moreover, electron-withdrawing substituents were found to reduce the polymerisation rate and chain propagation, resulting in lower activities and polymer molecular weights. The high melting temperatures of obtained polyethylene (above 130 °C) confirmed a highly linear microstructure, as further verified by high-temperature NMR measurements. The use of hybrid steric hindrance in these C_2-symmetric iron precatalysts not only rendered them highly active but also produced high molecular weight polyethylene, making them distinct from previously reported symmetrical iron complexes for ethylene polymerisation.

Data availability

The data supporting this article have been included as part of the ESI.†

Conflicts of interest

There are no conflicts to declare.

Acknowledgements

Notes and references

1 (a) Z. Flisak and W.-H. Sun, *ACS Catal.*, 2015, **5**, 4713–4724; (b) Y. Wang, R. Gao, Q. Gou, J. Lai, R. Zhang, X. Li and Z. Guo, *Eur. Polym. J.*, 2022, **181**, 111693; (c) N. E. Mitchell and B. K. Long, *Polym. Int.*, 2019, **68**, 14–26; (d) Z. Ma, W. Yang and W.-H. Sun, *Chin. J. Chem.*, 2017, **35**, 531–540.

2 (a) Y. Champouret, O. H. Hashmi and M. Visseaux, *Coord. Chem. Rev.*, 2019, **390**, 127–170; (b) L. Jasinska-Walc, M. Bouyahyi and R. Duchateau, *Acc. Chem. Res.*, 2022, **55**, 1985–1996.

3 (a) G. J. P. Britovsek, V. C. Gibson, B. S. Kimberley, P. J. Maddox, S. J. McTavish, G. A. Solan, A. J. P. White and D. J. Williams, *Chem. Commun.*, 1998, 849–850; (b) B. L. Small, M. Brookhart and A. M. A. Bennett, *J. Am. Chem. Soc.*, 1998, **120**, 4049–4050.

4 (a) C. Bianchini, G. Giambastiani, I. G. Rios, G. Mantovani, A. Meli and A. M. Segarra, *Coord. Chem. Rev.*, 2006, **250**, 1391–1418; (b) T. Xiao, W. Zhang, J. Lai and W.-H. Sun, *C. R. Chim.*, 2011, **14**, 851–855; (c) Z. Wang, G. A. Solan, W. Zhang and W.-H. Sun, *Coord. Chem. Rev.*, 2018, **363**, 92–108; (d) V. C. Gibson, C. Redshaw and G. A. Solan, *Chem. Rev.*, 2007, **107**, 1745–1776; (e) W. Zhang, W.-H. Sun and C. Redshaw, *Dalton Trans.*, 2013, **42**, 8988–8997.

5 (a) Z. Wang, G. A. Solan, W. Zhang and W.-H. Sun, *Coord. Chem. Rev.*, 2018, **363**, 92–108; (b) J. Ma, C. Feng, S. Wang, K. Q. Zhao, W.-H. Sun, C. Redshaw and G. A. Solan, *Inorg. Chem. Front.*, 2014, **1**, 14–34.

6 W.-H. Sun, S. Jie, S. Zhang, W. Zhang, Y. Song, H. Ma and J. Chen, *Organometallics*, 2006, **25**, 666–677.

7 (a) V. C. Gibson and G. A. Solan, *Top. Organomet. Chem.*, 2009, **26**, 107–158; (b) V. C. Gibson and G. A. Solan, *Catal. Without Prec. Metals*, 2010, pp. 111–141.

8 (a) S. Jie, S. Zhang, W.-H. Sun, X. Kuang, T. Liu and J. Guo, *J. Mol. Catal. A: Chem.*, 2007, **269**, 85–96; (b) J. Guo, Q. Chen, W. Zhang, T. Liang and W.-H. Sun, *J. Organomet. Chem.*, 2021, **936**, 121713; (c) M. Zhang, W. Zhang, T. Xiao, J.-F. Xiang, X. Hao and W.-H. Sun, *J. Mol. Catal. A: Chem.*, 2010, **320**, 92–96; (d) S. Jie, S. Zhang and W.-H. Sun, *Eur. J. Inorg. Chem.*, 2007, **2007**, 5584–5598.

9 (a) W. Zhang, W. Chai, W.-H. Sun, X. Hu, C. Redshaw and X. Hao, *Organometallics*, 2012, **31**, 5039–5048; (b) R. Zhang, M. Han, I. V. Oleynik, G. A. Solan, I. I. Oleynik, Y. Ma, T. Liang and W.-H. Sun, *Appl. Organomet. Chem.*, 2021, **35**, e6376; (c) F. Huang, Q. Xing, T. Liang, Z. Flisak, B. Ye, X. Hu, W. Yang and W.-H. Sun, *Dalton Trans.*, 2014, **43**, 16818–16829; (d) Y. Zhang, H. Suo, F. Huang, T. Liang, X. Hu and W.-H. Sun, *J. Polym. Sci., Part A: Polym. Chem.*, 2017, **55**, 830–842.

10 (a) V. K. Appukuttan, Y. Liu, B. C. Son, C.-S. Ha, H. Suh and I. Kim, *Organometallics*, 2011, **30**, 2285–2294; (b) C.

2040 | *React. Chem. Eng.*, 2025, **10**, 2030–2042

This journal is © The Royal Society of Chemistry 2025

Bariashir, Z. Wang, Y. Ma, A. Vignesh, X. Hao and W.-H. Sun, *Organometallics*, 2019, **38**, 4455–4470; (*c*) Z. Wang, R. Zhang, W. Zhang, G. A. Solan, Q. Liu, T. Liang and W.-H. Sun, *Catal. Sci. Technol.*, 2019, **9**, 1933–1943.

11 (*a*) V. C. Gibson and G. A. Solan, *Organomet. Chem.*, 2009, **26**, 107–158; (*b*) V. C. Gibson and G. A. Solan, *Catal. Without Prec. Metals*, 2010, pp. 111–141.

12 (*a*) A. Razzaq, Y. Ma, Q. Mahmood, Z. Hu, Y. Wang, S. Zou, A. Zhou, T. Liang, S. Kong and W.-H. Sun, *Eur. J. Inorg. Chem.*, 2024, e202400380; (*b*) K. F. Tahir, Y. Ma, Q. Mahmood, Y. Wang, G. Ren, S. Zou, H. Saeed, T. Liang and W.-H. Sun, *Polymer*, 2024, **308**, 127335; (*c*) S. Wang, B. Li, T. Liang, C. Redshaw, Y. Li and W.-H. Sun, *Dalton Trans.*, 2013, **42**, 9188–9197.

13 (*a*) W. Zhao, J. Yu, S. Song, W. Yang, H. Liu, X. Hao, C. Redshaw and W.-H. Sun, *Polymer*, 2012, **53**, 130–137; (*b*) C. Bariashir, Q. Y. Zhang, B. Ulambayar, G. A. Solan, T. L. Liang and W.-H. Sun, *Chin. J. Polym. Sci.*, 2023, **42**, 188–201; (*c*) M. Han, I. I. Oleynik, Y. Ma, I. V. Oleynik, G. A. Solan, X. Hao and W.-H. Sun, *Eur. J. Inorg. Chem.*, 2022, e202200224; (*d*) W. Zhang, S. Wang, S. Du, C. Y. Guo, X. Hao and W.-H. Sun, *Chem. Phys.*, 2014, **215**, 1797–1809; (*e*) Q. Zhang, Z. Zuo, Y. Ma, T. Liang, X. Yang and W.-H. Sun, *Dalton Trans.*, 2022, **51**, 8290–8302; (*f*) S. F. Yuan, Z. Fan, M. Han, Y. Yan, Z. Flisak, Y. Ma, T. Liang and W.-H. Sun, *Eur. J. Inorg. Chem.*, 2021, 1571–1580.

14 (*a*) J. Yu, H. Liu, W. Zhang, X. Hao and W.-H. Sun, *Chem. Commun.*, 2011, **47**, 3257–3259; (*b*) W.-H. Sun, W. Zhao, J. Yu, W. Zhang, X. Hao and C. Redshaw, *Chem. Phys.*, 2012, **213**, 1266–1273; (*c*) T. Liu, Y. Ma, G. A. Solan, Y. Sun and W.-H. Sun, *New J. Chem.*, 2023, **47**, 5786–5794; (*d*) T. Liu, Y. Ma, G. A. Solan, T. Liang and W.-H. Sun, *Appl. Organomet. Chem.*, 2021, **35**, e6259; (*e*) Q. Mahmood, J. Guo, W. Zhang, Y. Ma, T. Liang and W.-H. Sun, *Organometallics*, 2018, **37**, 957–970; (*f*) Q. Zhang, R. Zhang, M. Han, W. Yang, T. Liang and W.-H. Sun, *Dalton Trans.*, 2020, **49**, 7384–7396; (*g*) X. Cao, F. He, W. Zhao, Z. Cai, X. Hao, T. Shiono, C. Redshaw and W.-H. Sun, *Polymer*, 2012, **53**, 1870–1880; (*h*) Q. Mahmood, E. Yue, J. Guo, W. Zhang, Y. Ma, X. Hao and W.-H. Sun, *Polymer*, 2018, **159**, 124–137; (*i*) R. Zhang, M. Han, Y. Ma, G. A. Solan, T. Liang and W.-H. Sun, *Dalton Trans.*, 2019, **48**, 17488–17498; (*j*) M. Liu, Z. Ning, Y. Ma, G. A. Solan, T. Liang and W.-H. Sun, *Organomet. Chem.*, 2023, **994**, 122740; (*k*) M. Zada, Q. Zhang, Q. Mahmood, Y. Ma, Y. Sun and W. H. Sun, *Dalton Trans.*, 2025, **54**, 7676–7689.

15 Y. Zhang, C. Wang and Z. Jian, *Eur. Polym. J.*, 2020, **128**, 109605.

16 (*a*) Z. Cheng, H. Gao, Z. Qiu, H. Zheng, D. Li, L. Jiang and H. Gao, *ACS Catal.*, 2024, **14**, 7956–7966; (*b*) H. Gao, Z. Cheng, G. Tu, Z. Qiu, X. Xiao, H. Zhou, H. Zheng and H. Gao, *Chin. Chem. Lett.*, 2025, **36**, 110762; (*c*) C. Bariashir, Z. Wang, H. Suo, M. Zada, G. A. Solan, Y. Ma, T. Liang and W.-H. Sun, *Eur. Polym. J.*, 2019, **110**, 240–251; (*d*) C. Bariashir, Z. Wang, G. A. Solan, C. Huang, X. Hao and W.-H. Sun, *Polymer*, 2019, **171**, 87–95; (*e*) H. Suo, I. I. Oleynik, C. Bariashir, I. V. Oleynik, Z. Wang, G. A. Solan, Y. Ma, T. Liang and W.-H. Sun, *Polymer*, 2018, **149**, 45–54.

17 Z. Wang, G. A. Solan, Q. Mahmood, Q. Liu, Y. Ma, X. Hao and W.-H. Sun, *Organometallics*, 2018, **37**, 380–389.

18 (*a*) D. C. Crans, M. L. Tarlton and C. C. McLauchlan, *Eur. J. Inorg. Chem.*, 2014, 4450–4468; (*b*) K. F. Tahir, Y. Ma, Q. Mahmood, G. Ren, A. Khalid, Y. Wang, S. Zou, T. Liang and W.-H. Sun, *Precis. Chem.*, 2024, **2**, 655–668; (*c*) Q. Mahmood, Y. Ma, X. Hao and W.-H. Sun, *Appl. Organomet. Chem.*, 2019, e4857.

19 (*a*) B. L. Small and M. Brookhart, *J. Am. Chem. Soc.*, 1998, **120**, 7143–7144; (*b*) G. J. P. Britovsek, M. Bruce, V. C. Gibson, B. S. Kimberley, P. J. Maddox, S. Mastroianni, S. J. McTavish, C. Redshaw, G. A. Solan, S. Stromberg, A. J. P. White and D. J. Williams, *J. Am. Chem. Soc.*, 1999, **121**, 8728–8740.

20 (*a*) L. Falivene, R. Credendino, A. Poater, A. Petta, L. Serra, R. Oliva, V. Scarano and L. Cavallo, SambVca 2, *Organometallics*, 2016, **35**, 2286–2293; (*b*) L. Falivene, L. Cavallo and G. Talarico, *ACS Catal.*, 2015, **5**, 6815–6822.

21 X. Li, L. Qin, Q. Mahmood, Z. Yu, S. Zou, Y. Wang, T. Liang and W.-H. Sun, *Eur. Polym. J.*, 2023, **200**, 112520.

22 (*a*) M. Xu, Y. Liu, W. Pang, Y. Pan, M. Chen, C. Zou and C. Tan, *Polymer*, 2022, **255**, 125116; (*b*) Q. Wang, Z. Zhang, C. Zou and C. Chen, *Chin. Chem. Lett.*, 2022, **33**, 4363–4366.

23 (*a*) A. K. Tomov, V. C. Gibson, G. J. P. Britovsek, R. J. Long, M. van Meurs, D. J. Jones, K. P. Tellmann and J. J. Chirinos, *Organometallics*, 2009, **28**, 7033–7040; (*b*) L.-H. Guo, H.-Y. Gao, L. Zhang, F.-M. Zhu and Q. Wu, *Organometallics*, 2010, **29**, 2118–2125.

24 (*a*) G. J. P. Britovsek, S. Mastroianni, G. A. Solan, S. P. D. Baugh, C. Redshaw, V. C. Gibson, A. J. P. White, D. J. Williams and M. R. J. Elsegood, *Chem. – Eur. J.*, 2000, **6**, 2221–2231; (*b*) G. J. P. Britovsek, V. C. Gibson, B. S. Kimberley, S. Mastroianni, C. Redshaw, G. A. Solan, A. J. P. White and D. J. Williams, *J. Chem. Soc., Dalton Trans.*, 2001, 1639–1644.

25 (*a*) L. S. Lee, H. J. Ou and H. F. Hsu, *Fluid Phase Equilib.*, 2005, **231**, 221–230; (*b*) Q. Mahmood, Y. Ma, X. Hao and W. H. Sun, *Appl. Organomet. Chem.*, 2019, **33**, e4857; (*c*) C. Huang, A. Vignesh, C. Bariashir, Q. Mahmood, Y. Ma, Y. Sun and W. H. Sun, *J. Polym. Sci., Part A: Polym. Chem.*, 2019, **57**, 1049–1058.

26 L. Deng, P. Margl and T. Ziegler, *J. Am. Chem. Soc.*, 1999, **121**, 6479–6487.

27 Á. Cartes, A. Rodríguez-Delgado, P. Palma, L. J. Sánchez and J. Cámpora, *Catal. Sci. Technol.*, 2014, **4**, 2504–2507.

28 L. M. Thierer, S. E. Jenny, V. Shastri, M. R. Donley, L. M. Round, N. A. Piro, W. S. Kassel, C. L. Brown, T. J. Dudley and D. L. Zubris, *J. Organomet. Chem.*, 2020, **924**, 121456.

29 (*a*) T. Zhang, D. Guo, S. Jie, W. H. Sun, T. Li and X. Yang, *J. Polym. Sci., Part A: Polym. Chem.*, 2004, **42**, 4765–4774; (*b*) W. Yang, J. Yi and W.-H. Sun, *Macromol. Chem. Phys.*, 2015, **216**, 1125–1133; (*c*) J. Dai and S. Dai, *Dalton Trans.*, 2024, **53**, 9268–9293.

This journal is © The Royal Society of Chemistry 2025

React. Chem. Eng., 2025, **10**, 2030–2042 | **2041**

30 (*a*) W. Zhang, P. M. Waddell, M. A. Tiedemann, C. E. Padilla, J. Mei, L. Chen and B. P. Carrow, *J. Am. Chem. Soc.*, 2018, **140**, 8841–8850; (*b*) Q. Mahmood, Y. Zeng, X. Wang, Y. Sun and W.-H. Sun, *Dalton Trans.*, 2017, **46**, 6934–6947; (*c*) X. Li, Z. Hu, Q. Mahmood, Y. Wang, S. Sohail, S. Zou, T. Liang and W. H. Sun, *Dalton Trans.*, 2024, **53**, 18193–18206.

31 (*a*) A. Khalid, Z. Hu, Y. Ma, Q. Mahmood, G. Ren, A. Razzaq, Y. Wang, T. Liang and W.-H. Sun, *Eur. Polym. J.*, 2024, **223**, 113635; (*b*) H. Saeed, K. F. Tahir, Q. Mahmood, R. Yuan, Y. Wang and W.-H. Sun, *ChemCatChem*, 2024, e202401640.

32 (*a*) G. W. Coates and R. M. Waymouth, *Science*, 1995, **267**, 217–219; (*b*) F. Zhai and R. F. Jordan, *Organometallics*, 2017, **36**, 2784–2799.

33 C. G. de Souza, R. F. de Souza and K. Bernardo-Gusmão, *Appl. Catal., A*, 2007, **325**, 87–90.

34 A. Bocian, M. Skrodzki, M. Kubicki, A. Gorczynski, P. Pawluc and V. Patroniak, *Appl. Catal., A*, 2020, **602**, 117665.